JOURNAL OF Materials CHEMISTRY

Synthesis of Ni metal particles by reaction between bis(cyclooctadiene)nickel(0) and sol–gel SiO_2 modified with Si–H groups.

Sandra Dirè,*[a] Riccardo Ceccato,[a] Giacomo Facchin[b] and Giovanni Carturan[a]

[a]*Dipartimento di Ingegneria dei Materiali, Università di Trento, via Mesiano 77, 38050 Trento, Italy. E-mail: Sandra.Dire@ing.unitn.it*
[b]*Centro di Chimica Metallorganica del CNR, Istituto di Chimica Industriale, Facoltà di Ingegneria, Università di Padova, via Marzolo 9, 35131 Padova, Italy*

Received 25th July 2000, Accepted 2nd October 2000
First published as an Advance Article on the web 5th January 2001

Ni–silica composites have been prepared by reacting the zerovalent nickel complex bis(cyclooctadiene)nickel(0), $Ni(cod)_2$, with triethoxysilane, methyltriethoxysilane, and tetraethoxysilane mixtures engaged in the gelling process. Nickel particles have been produced within the silica matrix at low temperature. Samples were prepared, changing the ratio between the silica precursors, the metal load, and the synthesis conditions. XRD, FTIR, TGA and N_2 adsorption data suggest the mechanism for the production of nickel particles is based on hydrosilylation of the Si–H moiety of triethoxysilane and Ni(0)-coordinated olefin, ensuring extreme dispersion of the reduced metal. The effect of thermal treatment on the silica matrix and metal dispersion has been studied; in case of triethoxysilane-derived matrices, the average size of the Ni particles is slightly modified by the pyrolysis process, carried out under argon up to 1000 °C. The features of the silica matrix are affected by the Ni dispersion, which changes the Si–O–Si bonding population, the surface area, the porosity and the pyrolysis behavior of the silsesquioxane gel.

Introduction

Metal particles dispersed in an inorganic oxide can be obtained by various physical and chemical techniques, including metal evaporation, decomposition of metal compounds and photochemical or chemical reduction of metal complexes.[1–7]

The properties of ultra-fine metal dispersions have attracted great attention, particularly for sol–gel-derived materials. A variety of oxide-based composites having technologically important optical, mechanical and electronic features may be prepared by the sol–gel process,[8] which allows the preparation of hybrid organic–inorganic materials by processing, under mild conditions, modified alkoxysilanes $R_xSi(OR')_{4-x}$ (R = organic function). The chemical nature of R groups, behaving as functional or polymerizable species, leads to interesting modifications of the material's features.[9,10]

Different methods have been used to prepare metal dispersions in sol–gel materials: impregnation of the porous xerogels, addition of metal precursor to the sol before gelling, and direct anchoring of metal complexes to functionalized metal alkoxides.[5–7,11–19] These approaches usually require a sequence of high temperature treatments after gel formation, calcination in air to decompose the metal compounds, for example, or reduction at high temperature by molecular hydrogen. These treatments may alter the xerogel's features and may favour the increase of the dimensions of the metal particles.

Hydrosilanes, like $HSi(OR)_3$, are versatile precursors for the synthesis of modified silica networks and display reductive ability due to the reactivity of the Si–H bond, such that they may be exploited for low temperature metal reduction with the aim of producing high metal dispersions.[20–22]

We report here the sol–gel synthesis and characterization of Ni–SiO_2 composites prepared from bis(cyclooctadiene)-nickel(0), $Ni(cod)_2$, and triethoxysilane (TREOS) and tetraethoxysilane (TEOS) mixtures. The possible interaction between the olefinic nickel complex and the Si–H groups of the TREOS precursor was considered a favourable factor in helping to produce high nickel dispersions in SiO_2.

Experimental

Preparation of samples

Commercially available reagents were used for the syntheses without any further purification. Bis(cyclooctadiene)nickel(0) was prepared and purified according to the literature method.[23] The yellow solid was kept in a Schlenk tube under nitrogen and added as a powder to the sol–gel mixtures.

NiT^H(I). A mixture of TREOS, tetrahydrofuran (THF), and distilled water in 1 : 4 : 3 molar ratios was reacted at 60 °C for 90 min under nitrogen in a 100 ml two-necked flask equipped with a reflux condenser. The solution (total volume 56.7 ml) was left under stirring at room temperature for a further 30 min. $Ni(cod)_2$, in the appropriate amount to obtain 1 wt% Ni in the final material, was dissolved at 0 °C in the clear sol, giving a pale yellow solution. Gelation occurred in 5 min with a small amount of gas being evolved. The transparent yellow gel, kept under nitrogen, turned deep green, then brown and finally black. The powdered solid was dried at 25 °C under reduced pressure (1.3 Pa) for 72 h.

NiT^H(II). The mixture of TREOS, THF and distilled water used to prepare NiT^H(I) was stirred under nitrogen for 10 min at room temperature. Bis(cyclooctadiene)nickel(0), in an amount sufficient to obtain 1 wt% Ni in the final material, was dissolved at 0 °C into the sol. The transparent sol turned deep brown and gelled in 2 h, giving a black solid which was dried at 25 °C under reduced pressure (1.3 Pa) for 72 h.

 DOI: 10.1039/b006019o

Table 1 Synthesis conditions and gelling times for the samples prepared

Sample	Ni load/ wt%	Silicon precursor, % molar ratio	Temperature[a]/ °C	Time[a]/ min	Gelling time
$NiT^H(I)$	1	TREOS, 100	60	90	5 min
$NiT^H(II)$	1	TREOS, 100	25	10	2 h
NiT	1	MTES, 100	60	90	7 d[b]
NiQ/T^H	5	TEOS–TREOS, 80 : 20	25	120	2 d
T^H	—	TREOS, 100	25	10	2 d
Q/T^H	—	TEOS–TREOS, 80 : 20	25	120	7 d

[a]Conditions employed for the hydrolysis of silicon precursors. [b]Nickel precursor segregation.

NiT. Methyltriethoxysilane (MTES) was employed as a precursor for modified SiO_2 and was used as described for $NiT^H(I)$. After $Ni(cod)_2$ addition, under the experimental conditions described above, the clear sol did not produce a homogeneous gel and segregation of the metal compound was observed.

NiQ/T^H. TEOS and TREOS in an 8 : 2 molar ratio were dissolved under nitrogen in THF and hydrolyzed with 1 M HCl solution using a $Si : THF : H_2O$ molar ratio of 1 : 4 : 3 (total solution volume 53.2 ml). After 120 min at room temperature, the correct amount of $Ni(cod)_2$ needed to achieve 5 wt% Ni in the final material was added at 0 °C. The slow dissolution of the complex produced a clear yellow solution, which progressively turned dark gray. Sample gelation was complete in 2 days. The gel was dried at room temperature under vacuum (1.3 Pa) for 72 h.

T^H and Q/T^H. Samples were prepared starting from TREOS (T^H) and an 8 : 2 TEOS–TREOS molar mixture (Q/T^H) using the conditions employed for the preparation of $NiT^H(II)$ and NiQ/T^H, in THF solution and without metal addition. Samples were processed as described above.

Table 1 reports the experimental conditions used for the preparation of samples.

Characterization techniques

FTIR spectra were recorded in transmission mode in the 4000–400 cm^{-1} range from KBr pellets using a Nicolet 5DXC spectrometer (128 scans, 2 cm^{-1} resolution). Thermogravimetric analyses (TGA) were performed on a Netzsch STA 409 thermobalance. Measurements were carried out with 10 °C min^{-1} heating rate at 600 and 1000 °C, using 200 mg samples in 100 ml min^{-1} Ar flow. N_2 adsorption experiments were carried out at 77 K on an ASAP 2010 Micromeritics instrument. Gel samples and pyrolyzed samples were degassed below 1.3 Pa at 25 and 250 °C, respectively. Surface area was calculated by the BET equation in the interval $0.05 \leqslant p/p_0 \leqslant 0.33$ with a least-squares fit of 0.998. Total pore volume was calculated at $p/p_0 = 0.995$ and pore size distributions were obtained from absorption isotherms using the BJH model. XRD spectra were collected on a Rigaku DMax diffractometer in the Bragg–Brentano configuration, using Cu-Kα radiation and a monochromator on the diffracted beam. A modified Rietveld method program[24] was employed for the quantitative phase analyses and the evaluation of the average crystallite dimensions.

Results and discussion

In a previous study,[22] dispersions of various metals in sol–gel SiO_2 were obtained by dissolution of Ni, Cu and Co chlorides or nitrates into a gelling solution prepared starting from TREOS. The metal reduction did not take place at room temperature and H_2 treatment at 600 °C was required for reduction to metal. In the case of Ni, particles with an average size of 170 Å were obtained. In the same work,[22] 1 wt% Pt on silica was obtained at 25 °C starting from TREOS and $Pt(allyl)_2$, which is reduced by the Si–H groups to Pt particles of 10–20 Å in diameter. This fact suggested that organometallic rather than inorganic metal compounds should preferentially be used to prepare high metal dispersions in a sol–gel matrix. Moreover, this synthetic approach involves mild experimental conditions and assures maintenance of the original structural and surface features of xerogel networks.

Ni–silica composites are here prepared *via* the sol–gel process in a one step reaction at low temperature, taking advantage of the reactivity of the Si–H bond of TREOS towards olefinic complex of nickel(0). $Ni(cod)_2$ is rather stable and can be handled in air for short periods without noticeable decomposition.[25] The complex is insoluble in alcoholic solvents commonly used in the sol–gel synthesis and moderately soluble in tetrahydrofuran.

In order to define the metal load influence on the metal particle distribution, different amounts of nickel precursor (1 and 5 Ni wt%) were added to the silica-based sols. The reactivity of $Ni(cod)_2$ towards the forming SiO_2 gel network and its decomposition were investigated as a function of gelling conditions and of the molecular ratio of Si–H groups to $Ni(cod)_2$.

Fig. 1 presents the FTIR spectra of T^H, $NiT^H(I)$ and $NiT^H(II)$ xerogels. The spectrum of T^H shows signals at 3647 and 956 cm^{-1} due to Si–OH terminal units and at 2978 and 1400 cm^{-1} due to residual C–H bonds. The Si–H bonds give rise to peaks at 2260 and 840 cm^{-1}, due to Si–H stretching and bending vibrations, respectively (the latter are overlapped with the Si–O and Si–OEt signals). The Si–O bond vibrations occur at 1166, 1078, 890 and 455 cm^{-1}. It is noteworthy that there are important differences between the $NiT^H(I)$ and T^H spectra: the former shows a complex and large Si–O–Si band in the 1180–1000 cm^{-1} range, sharp signals at 2260 and 840 cm^{-1} due to Si–H bonds and definite peaks at 1262 and 830 cm^{-1}, not present in the T^H spectrum, assigned to the presence of Si–C(H) bonds.[26] These Si–C peaks are not present in the spectrum of $NiT^H(II)$, although the Si–O and Si–H signals are similar to those seen for $NiT^H(I)$. The presence of residual silanols is evidenced by the peaks at 3640 and 950 cm^{-1}.

The amount of terminal SiOH units is quite low for $NiT^H(I)$, suggesting a higher degree of condensation with respect to T^H. Indeed, higher temperature and longer hydrolysis times for $NiT^H(I)$ (Table 1) may favour a more complete hydrolysis of the alkoxide groups and subsequent condensation between

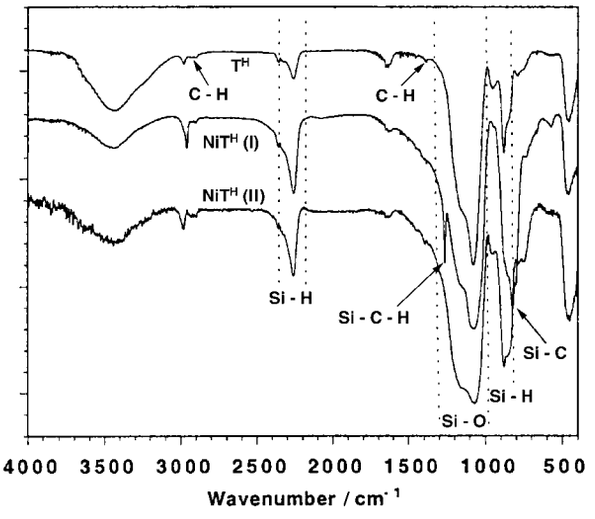

Fig. 1 FTIR spectra of T^H, $NiT^H(I)$ and $NiT^H(II)$.

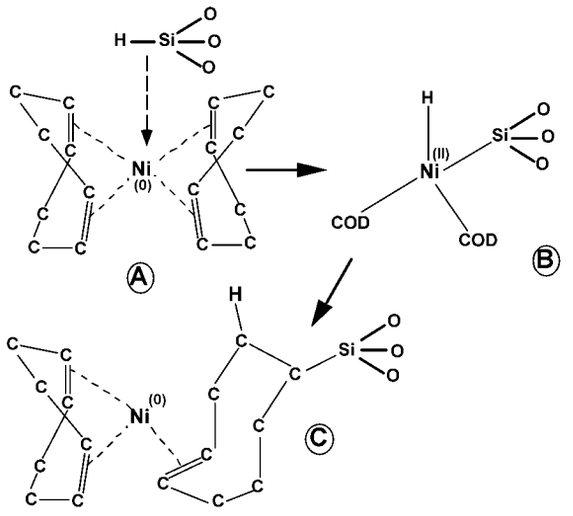

Scheme 1

silanols. The addition of $Ni(cod)_2$ has an important effect on the condensation rate, since the gelling time is much lower for $NiT^H(I)$ than for T^H (Table 1). This fact is evident even comparing the gelling times of T^H and $NiT^H(II)$, both prepared under the same hydrolysis conditions, but having quite different gelling times (Table 1).

From Fig. 1 spectra, the more important difference between $NiT^H(I)$ and $NiT^H(II)$ is the evidence of Si–C bond formation in $NiT^H(I)$: this fact suggests the occurrence of hydrosilylation between Si–H bonds and Ni(0)-coordinated olefins. Zerovalent nickel compounds are known to be effective catalysts for the addition reaction of hydrosilanes to olefins.[25,27] In the gelling solution, the mechanism of hydrosilylation may involve the classic oxidative addition of the silane $HSiX_3$ (X = O) to the metal to give **B**.[28] The subsequent rearrangement of this species to a σ-bonded Ni intermediate is followed by the transfer of silicon from the metal to the σ-bonded carbon atom,[28] leading to Si–C bond formation in intermediate species **C**, as shown in Scheme 1.

This reaction pathway should involve all the olefinic carbon bonds, ultimately leading to decomposition to Ni(0) aggregates. In the case of $NiT^H(I)$, addition of $Ni(cod)_2$ leads to immediate gelation (5 min), so that intermediate **C** remains trapped by the gel network, which may hinder complete decomposition, as observed in the case of $NiT^H(II)$, which has a gelling time of 120 min. However, the stability of **C** is limited: curing of

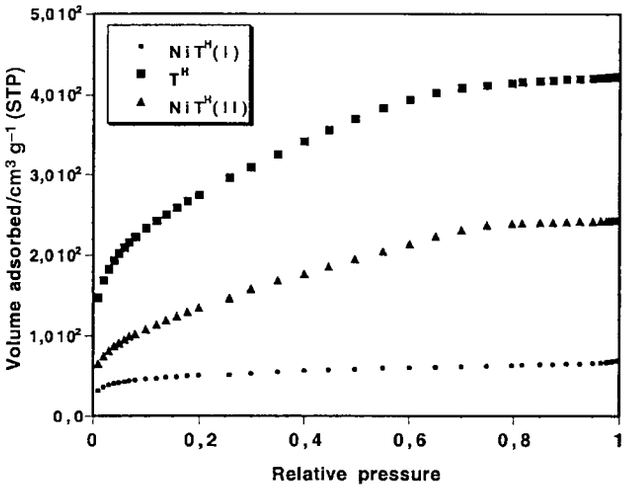

Fig. 2 N_2 adsorption isotherms of T^H and Ni–silica samples at different temperatures.

Table 2 N_2 sorption results of Ni–silica samples prepared at different temperatures

Sample	Temperature/ °C	Specific surface area[a]/$m^2\ g^{-1}$	Pore volume[b]/ $cm^3\ g^{-1}$	Average pore diameter[c]/Å
T^H	25	980	0.65	30
$NiT^H(I)$	25	175	0.11	32
	600	64	0.04	32
	1000	24	0.02	41
$NiT^H(II)$	25	511	0.37	29
Q/T^H	25	1	0.0018	76
NiQ/T^H	25	473	0.42	36

[a]BET equation. [b]Total pore volume calculated at $p/p_0 = 0.995$. [c]BJH Adsorption.

$NiT^H(I)$ at 50 °C leads to disappearance of Si–C bond vibrations.

The lower Si–H bond population in T^H may be attributed to the much longer gelling time, favouring a more pronounced Si–H consumption by reaction with water. On the contrary, in the case of Ni samples, the fast gelation may preserve a higher amount of Si–H groups.

Nitrogen adsorption data suggest that the silica matrix densification depends on the degree of condensation of the sol before metal addition. Fig. 2 presents the N_2 adsorption isotherms of T^H, $NiT^H(I)$ and $NiT^H(II)$; relevant specific surface areas (SSA), pore volumes (PV) and average pore diameters (APD) are reported in Table 2. $NiT^H(I)$ displays a type I isotherm, typical of microporous solids; the shape of the T^H isotherm is probably determined by the presence of micro and mesopores, in agreement with the high APD (70 Å). The SSA of $NiT^H(I)$ is markedly lower than for T^H, which displays an SSA similar to previously reported values for hydridosilsesquioxane xerogels.[29] $NiT^H(II)$ shows intermediate behavior (Fig. 2 and Table 2). These results indicate that the silsesquioxane network is modified by the reaction with the nickel precursor and agree with the FTIR Si–O–Si band width, in the interval 1180–1000 cm^{-1}, which is larger for $NiT^H(I)$ and $NiT^H(II)$ than for T^H.

The hydrosilylation reaction allows a molecular linkage between Ni species and the silsesquioxane backbone so that decomposition to metallic nickel is expected to generate a very high metal dispersion. This fact is crucial for obtaining the reduction to Ni metal through metal decomposition at low temperature: as a matter of fact, the process carried out using methyltriethoxysilane (NiT) does not produce a homogeneous gel after addition of $Ni(cod)_2$, which segregates without decomposition.

The XRD spectrum of $NiT^H(I)$ cured at 50 °C (Fig. 3) is characterized by haloes typical of the amorphous silsesquioxane phase with a weak signal at $2\theta = 44.9°$, due to fcc Ni. The $NiT^H(II)$ XRD spectrum shows the same features. The results of the profile fitting analyses of the XRD spectra[24,30] are reported in Table 3. $NiT^H(I)$ displays Ni crystallites 20 Å in diameter; quantitative estimation of the metal content indicates that it corresponds to the nominal 1 wt% Ni load and the calculated Ni cell parameter agrees with reported values. Transmission electron microscopy of $NiT^H(I)$ evidences Ni crystallites (in some cases present as twin crystallites) completely embedded in the siliceous matrix. This fact and the crystallite growth under the electron beam[15] makes difficult the observation of the xerogel samples. However, the *d*-spaces, calculated from selected area diffraction patterns, agree with the XRD results, confirming the presence of fcc Ni. After heat treatment at 600 °C in flowing Ar, the XRD spectrum of the sample remains unchanged, except for a moderate increase in the crystallite size (Table 3). Heating at 1000 °C produces sharp reflections at $2\theta = 44.9$ and 51.8° due to fcc Ni (Fig. 4) with the

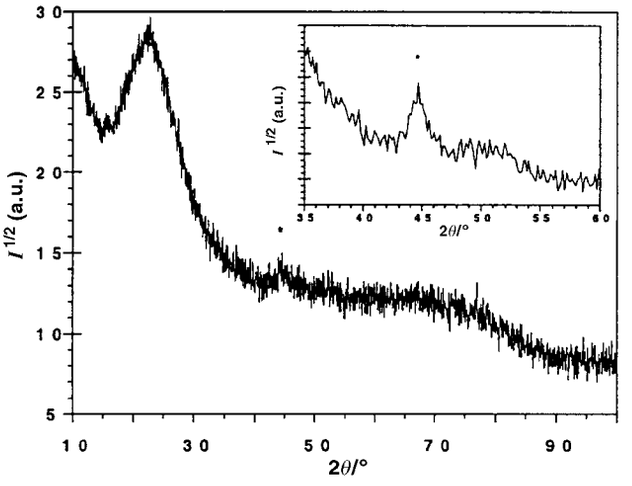

Fig. 3 XRD spectrum of NiT^H(I) cured at 50 °C. The magnification of the spectrum with the Ni fcc signal (*) is shown in the insert.

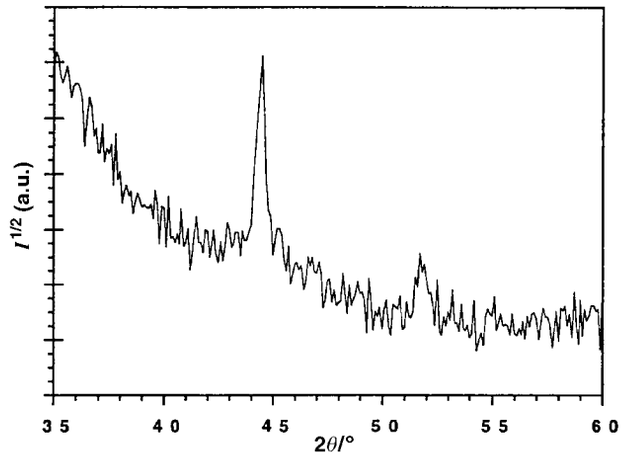

Fig. 4 XRD spectrum of 1 wt% Ni–SiO_2 composite pyrolyzed at 1000 °C.

amorphous silica halo at $2\theta = 22°$. At this temperature, the increase in the Ni crystallite sizes is moderate (< 100 Å).

The thermogravimetric analysis was used to follow the pyrolysis process under Ar up to 600 and 1000 °C. Pyrolysis at 1000 °C of NiT^H(I) leads to 6 wt% total weight loss, resulting from two main steps at 100–300 °C (3.9 wt%) and at 300–800 °C (2.3 wt%). The first weight loss is mainly due to release of water, alcohol, and solvent trapped in the porous gel network or evolved by Si–OH and Si–H condensation.[31] The second step is due either to residual condensation between terminal units or to transformation of the silsesquioxane matrix into a silica network with evolution of H_2 and silane.[32,33] Indeed, weak Si–H absorption vibrations are still present in the FTIR spectrum of NiT^H(I) heated at 600 °C; treatment at 1000 °C leads to an infrared spectrum typical of amorphous SiO_2 (Fig. 5). The total porosity progressively decreases with the thermal treatment, with nearly constant mean pore size (Table 2), according to the retention of the isotherm shape. The pyrolysis behavior of NiT^H(II) completely agrees with the results obtained for NiT^H(I).

The T^H thermal behavior involves a total weight loss of 14 wt% in the interval 60–800 °C; this weight loss tallies with the presence of residual Si–OH and SiOEt groups in the spectrum of the as-prepared material (Fig. 1), and the hypothesis that absence of $Ni(cod)_2$ leads to minor cross-linking.

The influence of total metal load on metal particle sizes may

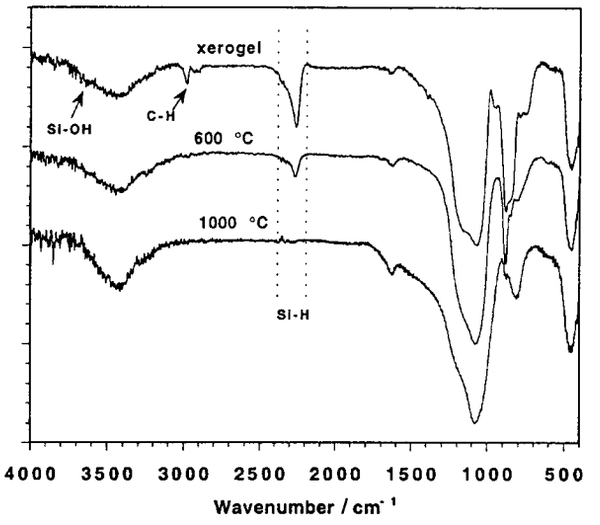

Fig. 5 NiT^H(II) FTIR spectral evolution with temperature. Analogous structural evolution is shown by NiT^H(I).

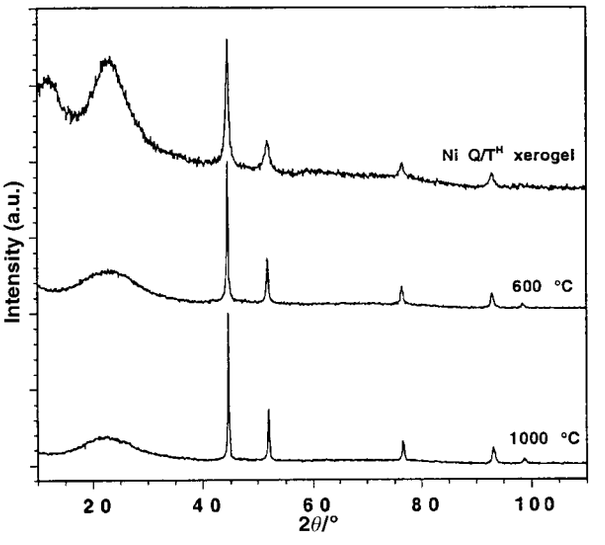

Fig. 6 Evolution of NiQ/T^H XRD spectra *vs.* temperature.

be deduced by comparison of NiT^H(I) and NiT^H(II) with the NiQ/T^H sample. The latter was prepared using a mixture of TEOS and TREOS providing the equivalent amount of Si–H to react with $Ni(cod)_2$. The XRD spectra of NiQ/T^H samples prepared at different temperatures are reported in Fig. 6. The xerogel spectrum shows the amorphous haloes due to silica and silsesquioxane phases and sharp peaks due to fcc Ni. The quantitative analysis (Table 3) confirms the nominal nickel load and the calculated cell parameter agrees with reported values. The crystallite size of the Ni particles is around 100 Å in the xerogel, and increases to 170 Å at 1000 °C, fcc Ni signals

Table 3 Rietveld profile fitting analyses of XRD spectra

Sample	Temperature/ °C	Phase fraction/ wt%	fcc Ni, a^a/Å	Crystallite size/Å
NiT^H(I)	50	1.0±0.1	$3.513\pm4\ 10^{-3}$	20±3
	600	1.0±0.1	$3.524\pm2\ 10^{-3}$	46±7
	1000	1.00±0.06	$3.514\pm1\ 10^{-3}$	85±10
NiT^H(II)	50	1.00±0.02	$3.519\pm9\ 10^{-3}$	13±1
NiQ/T^H	50	4.9±0.1	$3.5249\pm6\ 10^{-4}$	97±6
	600	5.15±0.07	$3.5233\pm1\ 10^{-4}$	120±2
	1000	5.84±0.07	$3.5211\pm1\ 10^{-4}$	170±4

[a]Standard nickel, a = 3.5238 Å.

Table 4 Weight losses and steps calculated from thermogravimetric curves

Sample	Total weight loss (%)	Temperature range/°C	Weight loss (%)
NiT^H(I)	6.2	100–300	3.9
		300–800	2.3
NiT^H(II)	8.1	100–300	3.9
		300–800	4.2
T^H	14.2	60–300	12.6
		300–800	1.6
NiQ/T^H	30.5	100–300	22
		300–800	7.9
Q/T^H	12.6	60–300	10.1
		300–800	2.5

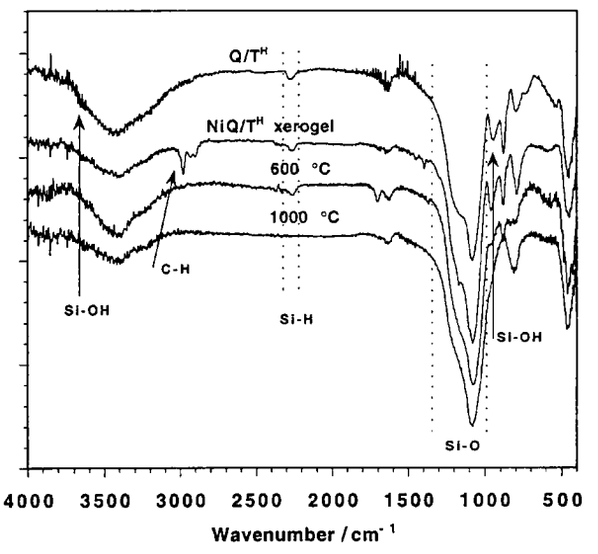

Fig. 7 NiQ/T^H thermal evolution followed by FTIR spectroscopy.

being sharper for samples heated at 600 and 1000 °C (Fig. 6). At 600 °C, the silsesquioxane phase has almost disappeared and the broad band of amorphous silica is present at $2\theta = 22.9°$. This evolution parallels the increase in the Ni metal fraction (Table 3), probably owing to the loss of silicon-based species as a consequence of redistribution reactions.

These results deserve some general comments. The NiT^H(I) and (II) samples constitute apparent examples demonstrating that coupling of a labile organometallic species with the reactive Si–H groups in TREOS-derived silica constitutes a steady approach to obtain extreme metal dispersions. The use of ordinary metal salts or the absence of the Si–H function requires severe experimental conditions and reduction mechanisms incompatible with homogeneously dispersed and very small metal particles. However, the physical state of the metallic crystallites at low temperature is essentially unstable and the hosting silica matrix must provide physical and chemical features suitable to prevent the collapse to a poor dispersion during the reduction and curing steps as well: a compact matrix, with a low content of terminal Si–OH and Si–OEt units, favours the formation and maintenance of high dispersions, as observed for NiT^H(I) and (II). However, accurate solution of organometallic species, TREOS hydrolysis and condensation, and experimental artifacts leading to a well textured Si–O–Si material are not enough for the purpose at hand, because the gelling process is sensitive to the organometal load, which, in its turn, is not innocent. As a matter of fact, the SSA of Q/T^H is 1 $m^2\ g^{-1}$ but increases to 473 $m^2\ g^{-1}$ for NiQ/T^H with a PV of 0.42 $cm^3\ g^{-1}$ *vs.* 0.0018 obtained for the parent Q/T^H sample. Consistently, it may be concluded that cultural intersection between sol–gel science and organometallic chemistry needs to develop a proper cultural space, otherwise the achievement of good results may be a fortunate event and not a logical expectation.

Turning to the data from the NiQ/T^H and Q/T^H samples, the TG analysis (Table 4) indicates a 30% total weight loss for NiQ/T^H: the weight loss (22%) recorded in the interval 100–300 °C is probably associated with release of water and products generated by condensation of SiOH and SiOEt, which are present in higher concentration in NiQ/T^H than in Q/T^H [see Fig. 7: ν(C–H) 3000–2900 cm^{-1}, ν(Si–OH) 3670 and 960 cm^{-1}]. The pyrolysis process leads to the conversion of the Si–H-modified network into a pure silica network, with the progressive disappearance of the Si–H bands (Fig. 7). Accordingly, the NiQ/T^H network is characterized by low crosslinking and high porosity, and behaves as a microporous solid, judging from the nitrogen adsorption results (Table 2). In contrast, Q/T^H is non porous. This fact can be related to the different gelling time and gel aging induced by the presence of Ni species, which are probably involved in reactions leading to decomposition to metal by mechanisms only in part involving hydrosilylation of $Ni(cod)_2$.

Conclusion

The reaction between bis(cyclooctadiene)nickel(0) and triethoxysilane at low temperature leads to a fine dispersion of Ni metal particles in the silica gel matrix. The experimental evidence for Si–C bond formation during the reaction suggests the occurrence of hydrosilylation between Si–H and Ni(0)-coordinated olefin. This reaction pathway assures the extreme dispersion of the reduced metal and leads to relevant structural changes in the gel network. The average size of the Ni particles is slightly modified by the pyrolysis process up to 1000 °C. The increase of the organometal load and the decrease of the Si–H group content lead to an increase in Ni particle size and to modification of the features of Ni–silica composites.

Acknowledgements

The financial support of CNR-PF MSTA II is gratefully acknowledged.

References

1 U. Kreibig and M. Vollmer, *Optical Properties of Metal Clusters*, Springer-Verlag Berlin, Heidelberg, 1995, pp. 207–234.
2 R. C. Davis and K. J. Klabunde, *Chem. Rev.*, 1982, **82**, 153.
3 G. A. Niklasson, *J. Appl. Phys.*, 1987, **62**, 258.
4 H. Bönnemann, W. Brijoux and T. Joussen, *Angew. Chem., Int. Ed. Engl.*, 1990, **29**, 273.
5 A. Chatterjee and D. Chakravorty, *J. Phys. D: Appl. Phys.*, 1989, **22**, 1386.
6 B. Breitscheidel, J. Zieder and U. Schubert, *Chem. Mater.*, 1991, **3**, 559.
7 C. Görsmann, U. Schubert, J. Leyrer and E. Lox, *Mater. Res. Soc. Symp. Proc.*, 1996, **435**, 625.
8 J. F. Brinker and G. W. Scherer, *Sol–Gel Science*, Academic Press, San Diego, CA, 1990.
9 H. Schmidt, *Mater. Res. Soc. Symp. Proc.*, 1990, **180**, 961 and references therein.
10 J. Wen and J. Wilkes, *Chem. Mater.*, 1996, **8**, 1667 and references therein.
11 R. Gomez, T. Lopez, V. Bertin, R. Silva, P. Salas and I. Schifter, *J. Sol–Gel Sci. Technol.*, 1997, **8**, 847.
12 H. Kozuka and S. Sakka, *Chem. Mater.*, 1993, **5**, 222.
13 V. Vendange, E. Tronc and P. H. Colomban, *J. Sol–Gel Sci. Technol.*, 1998, **11**, 299.
14 M. A. L Villegas, M. A. Garcia, J. Llopis and J. M. Fernandez Navarro, *J. Sol–Gel Sci. Technol.*, 1998, **11**, 251.
15 U. Werner, M. Schmit and H. Schmidt, *Mater. Res. Soc. Symp. Proc*, 1996, **435**, 637.
16 C. Ferrari, G. Predieri, A. Tiripicchio and M. Costa, *Chem. Mater.*, 1992, **4**, 243.

17 Y. Matsumura, K. Tanaka, N. Tode, T. Yazawa and M. Haruta, *J. Mol. Catal. A*, 2000, **152**, 157.
18 H. Yanagi, S. Mashiko, L. A. Nagahara and H. Tokumoto, *Chem. Mater.*, 1998, **10**, 1258.
19 G. Mitrikas, Y. Deligiannakis, C. C. Trapalis, N. Boukos and G. Kordas, *J. Sol–Gel Sci. Technol.*, 1998, **13**, 503.
20 J. M. Tour, S. L. Pendalwar and J. P. Cooper, *Chem. Mater.*, 1990, **2**, 647.
21 H. A. Ketelson, M. A. Brook, R. Pelton and Y. M. Heng, *Chem. Mater.*, 1995, **7**, 1376.
22 R. Campostrini and S. Dirè, in *Eurogel '92*, ed. S. Vilminot, IPCMS, Strasbourg, 1995, 307.
23 F. Guerrieri and G. Salerno, *J. Organomet. Chem.*, 1976, **114**, 339.
24 L. Lutterotti, P. Scardi and P. Maistrelli, *J. Appl. Crystallogr.*, 1992, **25**, 459.
25 P. W. Jolly and G. Wilke, *The Organic Chemistry of Nickel*, Academic Press, New York, 1975, vol. II, p. 69.
26 L. J. Bellamy *The Infra-Red Spectra of Complex Molecules*, Chapman and Hall, London, 1975, ch. 20.
27 I. Ojima, in *The Chemistry of the Organic Silicon Compounds*, ed. S. Patai and Z. Rappoport, J. Wiley & Sons, London, 1989, p. 1480.
28 *Adv. Organomet. Chem.*, 1979, **17**, 407.
29 G. D. Sorarù, G. D'Andrea, R. Campostrini and F. Babonneau, *J. Mater. Chem.*, 1995, **5**, 1363.
30 L. Lutterotti, R. Ceccato, R. Dal Maschio and E. Pagani, *Mater. Sci. Forum*, 1998, **278–281**, 87.
31 R. Campostrini, G. D'Andrea, G. Carturan, R. Ceccato and G. D. Sorarù, *J. Mater. Chem.*, 1996, **6**, 585.
32 V. Belot, R. J. P. Corriu, D. Leclercq, P. H. Mutin and A. Vioux, *J. Mater. Sci. Lett.*, 1990, **9**, 1052.
33 V. Belot, R. Corriu, D. Leclercq, P. H. Mutin and A. Vioux, *Chem. Mater.*, 1991, **3**, 1052.